Analytical Extrapolation of Land Surface Temperatures in Clairvoyantly Perceived Regions Using Remote Sensing: A Case Study of Moscow, Taif, Amman, and Abu Dhabi

***Lulah Aziz Alshehri* (*)**

Highlights:

- Valuable insights into the relationship between clairvoyance and land surface temperature (LST) in clairvoyantly perceived regions are provided, which has not been extensively studied before.
- A significant contribution to the field of remote sensing is made by the use of satellite imagery from different sources to analyze and extrapolate LST in these regions.
- The finding suggests that there is no thermal anomaly during clairvoyance events compared to other months, and that there is relative balance between the central point and its surrounding points, that there may be a natural explanation for clairvoyant experiences.

Abstract:

In order to comprehend the underlying mechanism and control of clairvoyance, extensive studies were conducted in clairvoyantly perceived regions. Nevertheless, the dynamics of land surface temperature (LST) in these regions have not been verified, despite their crucial role in energy exchange between the Earth's surface and the atmosphere. In this context, this research aims to analyze and extrapolate LST in several clairvoyantly perceived regions using various optical imagery from different satellite sources, with the purpose of investigating the temporal and spatial variations in LST in those areas. One of the key findings of this research is that during clairvoyance events, there is no thermal anomaly that differs significantly from other months. Furthermore, no statistically significant differences were found between the central point and its surrounding points in each clairvoyantly perceived region, indicating relative balance between the central point and its adjacent points. Finally, no statistically significant differences at the 0.05 level were observed between the days before and after the clairvoyance event, suggesting a relative equilibrium in LST for the days surrounding the observed LST during the clairvoyance event.

Keywords: Land Surface Temperatures, Clairvoyantly Perceived Regions, Remote Sensing, Satellite sources, Spatial variations.

(*) member of the International Remote Viewing Association and an independent researcher in parapsychology

Introduction:

LST is a crucial variable for exploring the interactions between the Earth's surface and the atmosphere, including surface material exchange, energy balance, and surface physical and chemical processes. LST typically exhibits significant spatiotemporal variations due to the influence of changes in land cover type, vegetation cover, surface soil moisture, soil texture, topographical factors, and weather conditions. Therefore, LST has been widely used in various environmental studies, such as monitoring and assessing the risks of fires, floods, droughts, hurricanes, and earthquakes. Understanding the spatiotemporal variability of LST and its measurement is essential for gaining insights into how LST differs in disaster-prone areas.

This study focuses on tracking LST in clairvoyantly perceived regions that have experienced previous disasters. By "clairvoyantly perceived regions," we refer to areas where some individuals with clairvoyant abilities have been able to predict disasters that have occurred in them."

Clairvoyance is defined as a phenomenon that does not adhere to the laws of physics that explain the principles of vision. It allows individuals to mentally access distant locations and "see" and "know" what is there, even if the conditions for conventional vision, as defined by the experiments conducted by figures such as Ibn Al-Haytham, Galileo, Newton, and others, are not met from a physical perspective (Morris, 1978). This phenomenon has been demonstrated by the ability of individuals to achieve mental access to remote places and gain "sight" and "knowledge" of what exists there (Targ & Puthoff, 2005). Williams) 2016) also defined clairvoyance as the ability to discover unusual information through the mind.

Researchers from diverse fields, ranging from anthropology to physics and beyond, have persistently examined the phenomenon of clairvoyance using scientific tools specific to their respective disciplines (Zingrone & Alvarado, 2015). They aim to understand the mechanics and workings of clairvoyance. Tuszynski (2020) asserts that the study of consciousness is not only a valid area for scientific research but also one of the fundamental scientific problems that remain unresolved in modern times. The enigma of consciousness challenges all traditional theories. Moreover, even the brain itself has not been fully discovered as of our current time (O'Shea, 2005).

Drawing from evidence available in the early 1930s, many medical scientists have sought to explore the relationship between the mind and clairvoyance. This exploration extends to various aspects, including the field of neuroscience, the involuntary human nervous system, skin conductance levels, photoplethysmographic heart rate measurements, photoplethysmographic blood volume measurements, sympathetic nervous system activity, heart-brain synchronization, increased vascular resonance, and the emission of electromagnetic radiation from humans. These emissions can be measured using infrared and ultraviolet radiation equipment (Radin, 2004; McCraty & Atkinson, 2014).

Similarly, within the realm of physics, a number of scientists have endeavored to study geomagnetic fluctuations and their potential connection to clairvoyance. This includes investigating the relationship between clairvoyance and geomagnetic activity, geomagnetic pulsations, electromagnetic shielding, Local Sidereal Time, and photons. Furthermore, research has explored the link between clairvoyance and Schumann resonance, a physical phenomenon occurring in the Earth's atmosphere. This resonance is related to electromagnetic frequencies resulting from interactions between atmospheric elements, soil, seas, living organisms, and humans (Road and Tw, 2008; Spottiswood, no date).

Hypothesis:

This study assumes the existence of a statistically significant relationship between LST in clairvoyantly perceived regions and the occurrence of events.

Previous Studies:

Here, we will present a selection of previous studies in which researchers examined the relationship between LST and natural disasters (earthquakes, volcanoes, tsunamis, floods) in different regions of the world, elucidating the extent of the increase in LST before and after these disasters.

- *Rehman et al. (2019)* conducted a study to analyze land cover patterns before, during, and after flooding in North Sindh using satellite data, the focus was on changes in LST and the Normalized Difference Vegetation Index (NDVI) during the study period. The study also observed various values attributed to land surface characteristics. The study utilized three images captured by the Landsat-8 OLI/TIRS satellite on April 11, 2015, August 17, 2015, and October 20, 2015. The results of the study indicated an increase in vegetation cover, along with climate changes that led to a rise in LST in the study area by approximately 2 degrees Celsius after the flood event (REHMAN et al., 2019).

- *Achmad et al. (2019)* explored the relationship between LST and water as an indicator in the urban area of Band Aceh, Indonesia. The study utilized Landsat 5 TM satellite images captured on March 8, 1998, and

Landsat 8 OLI/TIRS images from June 3, 2018. The results of the study revealed urban development in Band Aceh, Indonesia, due to changes in land use and increased surface temperature, negatively impacting water index change measurements (Achmad et al., 2019).

- *Huda et al. (2020)* studied the relationship between changes in LST following earthquakes that occurred on July 7, 2018 (ML = 4.73) and October 11, 2018 (ML = 3.77) in the Cimandiri fault. The study utilized images captured by the Landsat 8 satellite to determine LST using algorithms. The study's results revealed an increase in LST on the day preceding the earthquakes on July 7, 2018, by 6.56 degrees Celsius, and on October 11, 2018, by 7.02 degrees Celsius, respectively (Huda et al., 2020).
- *Munawar Shah et al. (2021)* conducted an analysis of thermal anomalies was carried out using the Moderate Resolution Imaging Spectroradiometer (MODIS) spectral data, which relies on LST. This analysis was conducted in three different sizes and shallow depths in Pakistan, focusing on anomalous conditions occurring within 10 days before and after a major earthquake. The study utilized maps illustrating LST obtained from MODIS spectral data to track changes in LST over the earthquake's epicenter. The results indicated that changes in LST led to a state of anomaly occurring 10 days before the earthquake, with slight anomalies observed 20-25 days prior to the earthquake. These findings emphasize the significance of anomalies as a key indicator within a short to medium timeframe preceding earthquakes (Shah et al., 2021).
- *Girona et al. (2021)* conducted a study titled "Large-scale thermal unrest of volcanoes for years prior to eruption." The aim of this study was to identify warning signs of volcanic eruptions, with a primary focus on thermal energy emissions from volcano vents. The study utilized data from long-wave infrared radiation (10.780-11.280 micrometers) collected by satellites, which were statistically analyzed. The results revealed that volcanoes can exhibit a series of thermal disturbances for several years before an eruption occurs. This serves as an early indicator of volcanic reactivation, enabling us to predict volcanic eruptions in advance using various geophysical and geochemical methods (Girona et al., 2021).
- *Mossbridge et al. (2022)* explored the concept of precognition and its relationship with the boundaries of time and space. The study aimed to conduct an experimental review and theoretical discussion of the phenomenon of precognition, examining the challenges and limitations in studying this phenomenon by reviewing previous evidence, theories, and literature related to precognition. The researcher employed a

descriptive approach to study the phenomenon and discuss it by examining scientific evidence from previous studies and suitable statistical numerical experiments for data analysis. The study's results indicate that precognition is a genuine phenomenon that can be observed and measured under controlled conditions. The strongest evidence for precognition comes from studies using physiological measures such as EEG or functional magnetic resonance imaging (fMRI) (Mossbridge, 2022).

- *Serena m. Roney (2010)* conducted a study to indicate there is a relationship between local geomagnetic activity and meditation and psi (parapsychological phenomena). The study also involved the development of a theoretical model to explain the observed effects. The authors discussed potential mechanisms through which local geomagnetic activity and meditation might influence psi performance, including the role of the pineal gland and the electromagnetic fields generated by the brain. They proposed a model in which meditation facilitates psi performance by modifying the electromagnetic fields of the brain, including the local geomagnetic field. The study is related to parapsychological phenomena as it seeks to explore the possible effects of meditation and local geomagnetic activity on psi performance, which encompasses these phenomena. The results of the study showed a statistical relationship between the effect size in precognition experiments and local time. While this relationship may appear superficial, previous research has confirmed its existence, supporting the hypothesis (SERENA M. RONEY, 2010).
- *Adrian (2008)* conducted a study to investigate the relationship between extrasensory perception (ESP) and Earth's geomagnetic activity. The researcher aimed to test the hypothesis suggesting that relatively variable components of geomagnetic activity and geomagnetic pulsations might influence extrasensory perception and local sidereal time. Adrian analyzed a database consisting of 343 ESP experiments conducted at centers in the United Kingdom. Measurements of local geomagnetic fields were taken at different time intervals. The first-time interval was one second and included 99 experiments, while the second time interval involved 5-second intervals with 244 experiments. Fast Fourier Transform was used to convert these measurements into energy. The study examined patterns of extrasensory perception (ESP) effects based on local sidereal time and pulse activity within the 0.2-0.5 Hz range. The significance of the study lies in exploring the potential role of Earth's geomagnetic activity in precognition and human perception and its potential effects on remote viewing, clairvoyance, and precognition, which are associated with ESP. The study's results provided new insights

into the links between ESP and Earth's geomagnetic activity. It was found that ESP succeeds primarily during periods of enhanced pulse activity within the 0.2-0.5 Hz range. The study's findings have implications for the fields of remote viewing, clairvoyance, and precognition, which are all associated with ESP (ADRIAN RYAN, 2008).

- *El-Borie (2021)* conducted a study to understand the joint effects of solar-magnetic terrestrial activities and the North Atlantic Oscillation (NAO) on Earth's temperatures. The study sought to provide a better understanding of the relationship between these two factors. The underlying idea is that the Earth's magnetic field may interact with the human brain in some way, and therefore, fluctuations in the magnetic field may affect cognitive processes. The scientific method used in the study involved data analysis from various sources, including solar-magnetic terrestrial data, NAO data, and global surface temperature data. The researcher used statistical methods to determine the relationships between these variables and assess their impact on global surface temperatures. The study's results indicated that both solar-magnetic terrestrial activities and NAO had a significant impact on global temperatures. It was found that solar-magnetic terrestrial activities had a greater impact on temperature changes on Earth's surface during periods of low NAO activity, while NAO had a more substantial impact during periods of high solar-magnetic terrestrial activity (El-Borie, 2021).

Comparing these results with Adrian's study, which suggests a relationship between extrasensory perception and Earth's magnetic activity, and El-Borie's findings, which suggest a relationship between solar-magnetic terrestrial activities and temperature changes on Earth, we can derive the following conclusions:

- Extrasensory perception has a direct proportional with Earth's magnetic activity.
- Solar-magnetic terrestrial activity has a direct proportional with temperature.

Therefore, it is possible to conclude:
Extrasensory perception has a direct proportional with temperature.

Study Boundaries:

The following cities were selected (Al-Taif, Amman, Moscow, Abu Dhabi) as shown in Figure (1) as samples for studying LST in clairvoyant regions. These areas serve as representative models for testing the primary hypothesis in this study. The chosen study areas were selected to encompass a diverse range of clairvoyant regions characterized by variations in environmental, climatic, social, and economic conditions. Additionally, satellite images were available before and after the clairvoyance events to track rapid temperature changes.

Methodology:

For this study, a combination of quasi-experimental and analytical methodologies was employed. The quasi-experimental approach, which is a subtype of Experimental Approach that does not control the independent variable and does not follow complete randomness in sample selection, was used. In contrast to true experimental approach, quasi-experimental approach considers equivalence in some aspects when choosing the study sample.

The quasi-experimental methodology was chosen as the most suitable for this study because it investigates the temporal and spatial detection of LST in clairvoyant regions, specifically the case study areas (Al-Taif, Amman, Moscow, Abu Dhabi).

Additionally, the analytical methodology was applied to deconstruct and evaluate various scientific issues related to the temporal and spatial detection of LST in clairvoyant regions within the same case study areas.

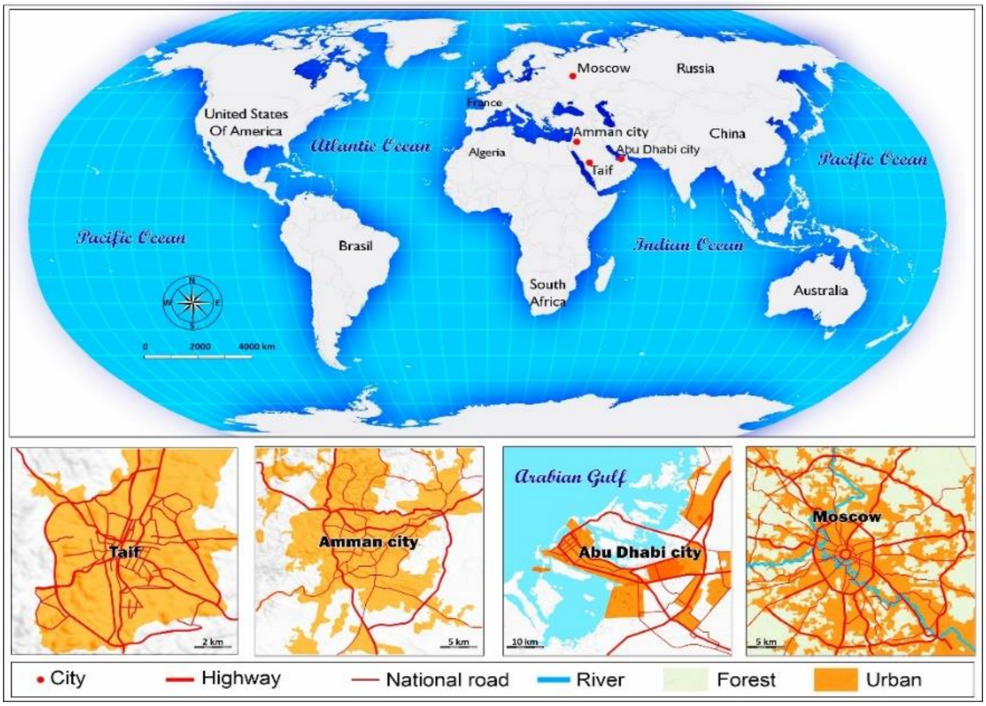

Figure (1). Map of Study area

Study Sample:

The study sample comprised four regions that were clairvoyantly perceived on specific dates, as indicated below:

- Abu Dhabi: Clairvoyance event observed on 2022-01-31.
- Amman: Clairvoyance event observed on 2016-05-25.

- Al-Taif: Clairvoyance event observed on 2018-05-09.
- Moscow: Clairvoyance event observed on 2018-06-05.

Region 1 (Al-Taif): The research area in Al-Taif is located at coordinates 40.419214 E and 21.288468 N. It is characterized by moderate temperatures, with the city's elevation above sea level significantly influencing its climate. Al-Taif is situated at an altitude of approximately 1450 meters. Temperature ranges from 28 to 22 degrees Celsius during the summer, while in winter, temperatures vary from 15 to 9 degrees Celsius (Comprehensive Urban Vision Report for Al-Taif, 2021).

Region 2 (Moscow): the research area in Moscow is located at coordinates 55.755826 N and 37.6173 E. It is situated within the southern taiga region and experiences a moderate continental climate with an average annual temperature of +5.8 degrees Celsius. The annual average rainfall in Moscow is 700 mm (Prokofyeva et al., 2021).

Region 3 (Amman): the study area in Amman is located at coordinates 36.035002 E and 32.018937 N. It is characterized by a Mediterranean climate, with a cold and wet winter extending from late September to the end of March. Rainfall varies throughout the winter season depending on geographical location, from year to year, and from place to place. Amman's winter season is marked by cold weather, with two weather patterns: polar dryness associated with the Siberian high-pressure system, leading to significant temperature drops, frost, and snow formation in some areas, and the second pattern, which involves cold, wet rain accompanying frontal depressions. Amman experiences its highest temperatures in July and August, while the lowest temperatures are recorded in January and February. Eastern winds from the Mediterranean Sea dominate Amman's climate, and in spring, the region is affected by the winds associated with the Khamsin depressions, which continue from mid-March to May (Amman Meteorology, Al-Najdawi, 2022).

Region 4 (Abu Dhabi): the research area in Abu Dhabi is located in Hamdan Street, northern Abu Dhabi, United Arab Emirates, with coordinates 24.493107 N and 54.367208 E. Abu Dhabi's climate is characterized by high temperatures, especially during the summer months. The emirate lies within the arid tropical zone, with the Tropic of Cancer crossing its southern half. High temperatures in the summer are associated with high relative humidity, particularly along the coast. Generally, Abu Dhabi experiences a mild winter with occasional rainfall throughout the year. Temperature can occasionally drop to low levels, and rain is infrequent (Statistics Center, 2017).

Data Collection Methods:

To achieve the research objectives, the study relied on the following tools to obtain data and information:

1. Secondary Sources: Information related to the theoretical aspect of the research was gathered from various secondary sources, including research papers, studies, articles, academic theses, and specialized scientific books in both Arabic and foreign languages relevant to the study's topic.
2. Primary Sources: Data related to the study was acquired through the following sources:
   - USGS (United States Geological Survey): The USGS website was used to access satellite imagery.
   - ESA Copernicus Open Access Hub: Satellite imagery was obtained from ESA Copernicus Open Access Hub.NASA (National Aeronautics and Space Administration): A portion of the imagery was sourced from NASA.

This study utilized three types of satellites to achieve the agreed-upon objectives:

- Landsat 8 and 9.
- Sentinel 3.
- Modis.

An effort was made to select satellite imagery that was cloud-free. Landsat imagery was acquired from the USGS website, while Sentinel imagery was obtained through ESA Copernicus Open Access Hub. Modis data was sourced from the National Aeronautics and Space Administration (NASA). The diversity in satellite sources was to obtain imagery on specific dates as well as ensure clear skies.

To compare the monthly and daily LST models in the clairvoyantly perceived regions, data from various satellites was used. These included images captured on the same date as the clairvoyance event and one image for each month over a year. Additionally, daily satellite imagery before and after the clairvoyance event was used to detect daily changes for ten days.

Data preparation involved using three software programs: GIS, Snap, and Google Earth.

The selection of satellite images was performed as follows:

- Acquiring satellite imagery for the day of the clairvoyance event by choosing the best imagery from the aforementioned satellites in terms of timing and cloud cover percentage. Cloud removal processes could obscure data beneath the clouds.
- Selecting satellite imagery for each month of the clairvoyance year.
- Choosing ten daily satellite images before the day on which clairvoyance occurred and ten daily images after the day on which clairvoyance occurred based on availability.

Research Methods and Tools:

Extraction of LST:

Before extracting LST, geometric correction was performed, andan appropriate coordinate system was applied to each region as follows:

- Al-Taif: WGS_1984_UTM_Zone_37N.
- Amman, Jordan: WGS_1984_UTM_Zone_36N.
- Abu Dhabi: WGS_1984_UTM_Zone_39N.
- Moscow: GCS_WGS_1984.

Subsequently, the study areas were truncated for all the visuals under study from satellites (Landsat, Sentinel and Modis) and for all ranges, using the geographic information system environment (ArcGIS).

Then, LST was derived in the four cities, with the extraction process differing based on the type of satellite. The following section will explain the procedure for each satellite separately.

Landsat 8 and 9 Satellites:

The LST can be estimated or calculated using the thermal bands of Landsat 8 and 9 satellites by applying a set of equations through a raster calculator in ArcMap. The first step involves extracting the indicators from the metadata file that comes with the satellite imagery when downloaded from the United States Geological Survey (USGS) website. The focus is primarily on Band 10 (thermal band), and Bands 4 and 5 to calculate the Normalized Vegetation Difference Index (NVDI).

It's worth noting that the calculated values of LST represent the top of the atmosphere (TOA), which is measured by the radiance of the blackbody, represented by three radiative values - one from the Earth's surface, one from the atmospheric layer, and the latter represents the radiance absorbed from space. The impact of the atmospheric layer usually appears around 1:0 Kelvin (Weng et al., 2004).

The goal here is to address the impact of the atmospheric layer in the research. This was done by selecting satellite imagery during clearsky periods with cloud cover less than 12% in the timeframes used for the study.

Extraction of LST from Landsat 8 and 9 Satellites:

Stage 1: In this stage, the digital values of satellite imagery are converted into spectral radiance values using the following equation (Tariq, et al. 2022):

- Calculate the Top of Atmosphere (TOA) Radiance:

$$TOA\,(L) = M_L * Q_{cal} + A_L$$

Where:

M_L is the multiplicative scaling factor for the band, obtained from the metadata file of the satellite image (RADIANCE_MULT_BAND_x, where x is the band number).

Q_{cal} is the digital number for Band 10.

A_L is the additive scaling factor for the band, also obtained from the metadata file of the satellite image (RADIANCE_ADD_BAND_x, where x is the band number).

Stage 2: Conversion to Brightness Temperature (B_T) In this stage, the spectral radiance (TOA(L)) is converted into brightness temperature (B_T) using the following equation:

$$B_T = \frac{K_2}{\ln\left(\frac{K_1}{L}\right) + 1} - 273.15$$

Where:

K_1 is the first thermal conversion constant, obtained from the metadata file of the satellite image (K_(1_CONSTANT_BAND_x), where x is the thermal band number).

K_2 is the second thermal conversion constant, obtained from the metadata file of the satellite image (K_(2_CONSTANT_BAND_x), where x is the thermal band number).

TOA(L) is the spectral radiance.

Stage 3: Deriving the Normalized Difference Vegetation Index (NDVI) In this stage, the Normalized Difference Vegetation Index (NDVI) is derived using the formula:

$$NDVI = \frac{Band_5 - Band_4}{Band_5 + Band_4}$$

Stage 4: Deriving the Proportion of Vegetation (P_v) The proportion of vegetation (P_v) is derived using the formula:

$$P_v = \left(\frac{NDVI - NDVI_{min}}{NDVI_{max} - NDVI_{min}}\right)^2$$

Where:
$NDVI_{max}$ is the maximum NDVI value.
$NDVI_{min}$ is the minimum NDVI value.

Stage 5: Deriving Spectral Emissivity (ε) In the final stage, the spectral emissivity (ε) is calculated. Emissivity represents the surface's ability to emit radiation compared to a blackbody at the same temperature. Emissivity values vary depending on the type, density, and growth stages of vegetation. For calculating surface emissivity:

$$\varepsilon = 0.004P_v + 0.989$$

Where:
P_v is the proportion of vegetation.

Stage 6: Calculating Land Surface Temperature To calculate (LST), it's necessary to correct the brightness temperature (BT) based on the emissivity values for different surface features. This correction is done using the following equation:

$$LST = \left(\frac{BT}{1 + \left(0.00115 * \frac{BT}{1.4388}\right) * Ln(\varepsilon)}\right)$$

Where:
BT is the brightness temperature.
ε is the emissivity.

Stage 7: Converting to Celsius (°C) To obtain the LST in degrees Celsius (°C), the absolute zero in Kelvin (K) is added to the result using the equation:

$$°C = LST - 273.15$$

Where:
LST is the land surface temperature.

Extracting LST from Sentinel Satellite (Sentinel 3):

Sentinel 3 products allow for the direct retrieval of LST using Algorithm 1, which is implemented internally through the open-source Sentinel Application Platform (SNAP). After obtaining LST for the studied cities, the data was exported as raster images using ArcGIS.

The formula for calculating LST from Sentinel 3 data is as follows:

$$LST = a_{f,i,pw} + b_{f,i}(T_{11} - T_{12})^{\frac{1}{\cos\left(\frac{\theta}{m}\right)}} + \left(b_{f,i} + c_{f,i}\right)T_{12} \ (1)$$

Extracting LST from MODIS Satellite:

For months and days when it was difficult to obtain LST data from Landsat and Sentinel 3 satellites, NASA data were used to access LST from MODIS products. To convert DN values to degrees Celsius, the following equation was applied:

$$\boldsymbol{LST = DN * 0.02 - 273.15}$$

Here, LST represents LST in degrees Celsius, and 0.02 is the measurement factor for MODIS LST products.

The Thermal Distribution of Clairvoyantly Perceived Regions and Their Surroundings:

To facilitate an understanding of the relationship between LST and clairvoyant regions, particularly the dynamics of LST, five buffer zones were created. These buffer zones serve to demarcate the central region, The central region encompasses the boundaries of the features that have been clairvoyantly perceived. The surrounding regions extend from distances of 5, 10, 15, and 20 units from the central point. They are named as follows:

- Central Point (CP): This zone contains the landmarks that have been clairvoyantly perceived.
- First Circle (C1): The first circle that extends beyond the central point.
- Second Circle (C2): The second circle that extends beyond the central point.
- Third Circle (C3): The third circle that extends beyond the central point.
- Fourth Circle (C4): The fourth circle that extends beyond the central point.

Figure (2) illustrates the buffer zone setup for reference.

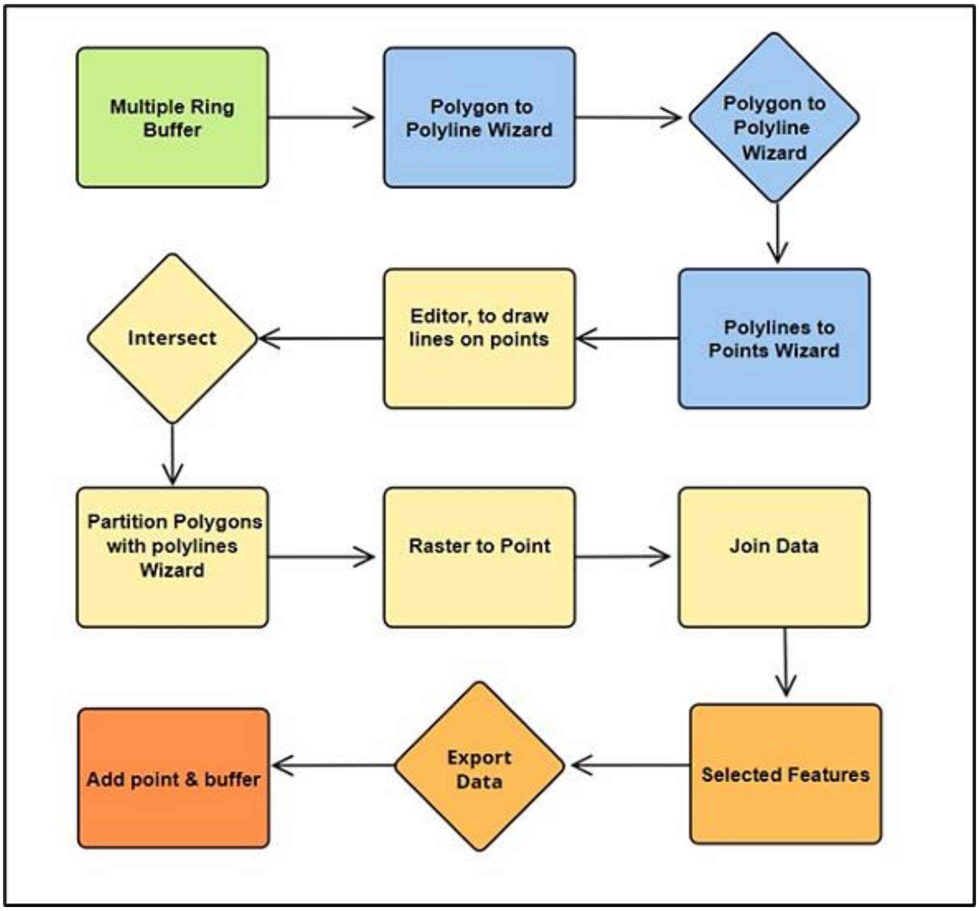

Figure (2): An illustrative diagram of the steps followed in creating the buffer zones

Drawing the temperature trend line:

To plot the trend of surface temperature increase, the following two steps were followed:

- The 'Summary Statistics' tool was used to obtain the mean for each ring. Afterward, the center of each part was extracted, and the line was drawn accordingly.

Statistical Methods Used for Temporal and Spatial Detection in the Research:

- The Kolmogorov-Smirnov normality test is employed to determine whether the data follows a normal distribution or not. This determination is made based on the significance level (p-value). If the p-value is greater than 0.05, it indicates that the data follows a normal distribution and vice versa. A normal distribution is a type of continuous probability distribution where most data points cluster around the center of the range, with the remainder tapering off symmetrically towards either end. The center of the range is also known as the mean of the distribution.

- Using measures of central tendency and dispersion, including arithmetic means, standard deviations, variances, and medians, to analyze the temporal and spatial aspects of surface temperature detection in the clairvoyantly perceived regions under investigation (Taif, Amman, Moscow, Abu Dhabi.
- The use of skewness is employed to measure the degree of asymmetry or deviation from symmetry in the data distribution. When a distribution is skewed to the right or has a positive skewness, it implies an asymmetrical distribution where most of the data points accumulate near the lower end of the range, with values decreasing as we move towards the upper end. In this case, the arithmetic mean is higher than the median, and positive skewness may occur due to the ease of the test or the selection of a distinguished sample, resulting in everyone achieving high scores. Conversely, if the curve is negatively skewed, it indicates a different distribution shape. Skewness helps assess the extent of data distribution asymmetry and identifies extreme values within the study's data.
- Kurtosis is used to measure the extent of distribution height, which is typically associated with the normal distribution. If a distribution has a high peak (greater than the normal distribution), it is said to be leptokurtic. If the distribution has a flat peak, it is said to be platykurtic. If the distribution peak is moderate (neither leptokurtic nor platykurtic), it is called mesokurtic. The expected value of kurtosis is approximately 3. This is observed in a symmetric distribution. Greater kurtosis values indicate positive kurtosis, which ranges from 1 to infinity. Conversely, lower kurtosis values indicate negative kurtosis, with a range from -2 to negative infinity. The higher the kurtosis value, the higher the peak, which helps assess the degree of data distribution inconsistency and identifies extreme values within the study's data.
- The Mann-Whitney non-parametric test was employed to assess the temporal and spatial detection of surface temperature in the observed regions of the study (Taif, Amman, Moscow, and Abu Dhabi). Additionally, it was used to test the presence of statistically significant differences in surface temperatures observed in the four regions on days before and after the day of observation. The Mann-

Whitney test was utilized to determine if the data in the study deviates from a normal distribution. Deviations from normal distributions are sometimes referred to as asymmetric or non-symmetric distributions, as they do not exhibit any form of symmetry. Symmetry means that one half of the distribution is the mirror image of the other half. For instance, the normal distribution is a symmetric distribution without skewness.

Results:

In this section of the research, the study's findings will be presented in five main categories:

- Monthly Temporal Variations of LST in the Central Point within the Clairvoyantly Perceived Regions.
- Relationships Between LST and Distance from the Central Point in the Clairvoyantly Perceived Regions and Surrounding Areas.
- Daily Temporal Variations of LST in the Central Point within the Clairvoyantly Perceived Regions.
- The Impact of Clouds on LST in the Clairvoyantly Perceived Regions.
- Analysis of the LST Gradient Compared to the day on which clairvoyance occurred.

- **Monthly Temporal Variations of LST in the Central Point within the Clairvoyantly Perceived Regions:**

- ***Abu Dhabi***

As shown in Figure (3), the LST in the Abu Dhabi region during the following months (June, September, July, and August) registers higher levels compared to the month in which clairvoyance occurred (January). In contrast, the months of February, March, April, May, October, November, and December record lower levels of LST compared to the month in which clairvoyance occurred (January). It is evident that most months throughout the year record lower LST levels compared to the month in which clairvoyance occurred. June recorded the highest LST with an average of 57.3993, while December recorded the lowest LST with an average of 20.8406.

Descriptive statistics for Abu Dhabi data:

Table (1) reveals that the average LST for the months in the Abu Dhabi region throughout the year was 45.1179 with a standard deviation of 13.53712. The median value was 51.0846, indicating that half of the year experiences LST reaching 51.0846. LST for the months of the year exhibited a left-skewed distribution with an average of 1.176 and a kurtosis value of -0.354, also left-skewed. The highest recorded LST was 57.40, while the lowest recorded temperature was 20.84. Furthermore, Table (2) regarding the Kolmogorov-Smirnov normality test demonstrates that the data does not follow a normal distribution, with a significance value of 0.003, 0.002 (sig < 0.05). Therefore, we reject the null hypothesis and accept the alternative hypothesis, indicating that the data does not follow a normal distribution.

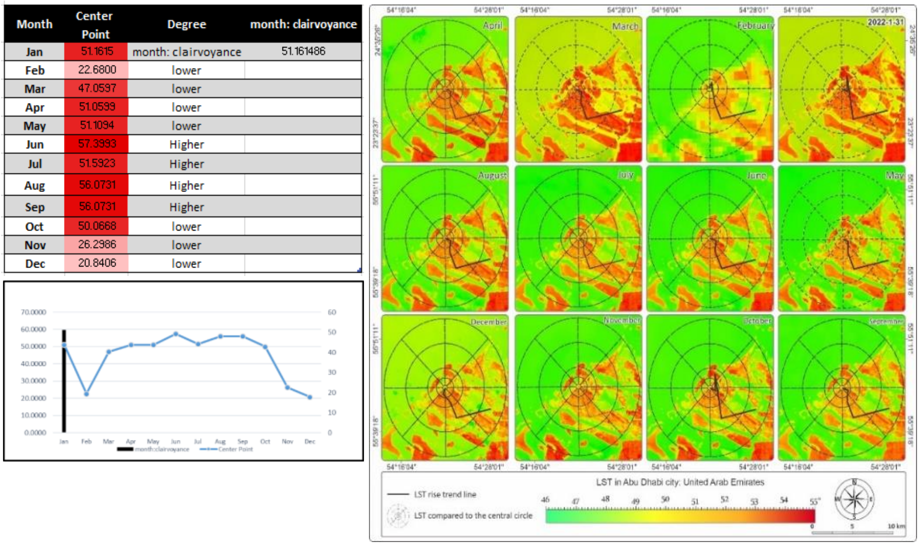

Figure (3): Monthly Temporal Maps of LST Changes Compared to the month in which clairvoyance occurred in Abu Dhabi city

Table (1): Descriptive statistics for LST in the city of Abu Dhabi

Descriptives				
			Statistic	**Std. Error**
Abu Dhabi	**Mean**		**45.1179**	**3.90783**
	95% Confidence Interval for Mean	**Lower Bound**	**36.5168**	
		Upper Bound	**53.7189**	
	5% Trimmed Mean		**45.7843**	
	Median		**51.0847**	
	Variance		**183.254**	
	Std. Deviation		**13.53712**	
	Minimum		**20.84**	
	Maximum		**57.4**	
	Range		**36.56**	
	Interquartile Range		**23.46**	
	Skewness		**-1.176**	**0.637**
	Kurtosis		**-0.354**	**1.232**

Table (2): the Kolmogorov-Smirnov normality test in the city of Abu Dhabi

Tests of Normality						
Abu Dhabi	Kolmogorov-Smirnov			Shapiro-Wilk		
	Statistic	df	Sig.	Statistic	df	Sig.
	0.309	12	0.002	0.752	12	0.003

- ***Amman***

As depicted in Figure (4), the LST in the Amman region during the following months (March, April, June, July, and August) record higher levels compared to the month in which clairvoyance occurred (May). Conversely, the months of January, February, September, October, November, and December register lower levels of LST compared to the month in which clairvoyance occurred (May).

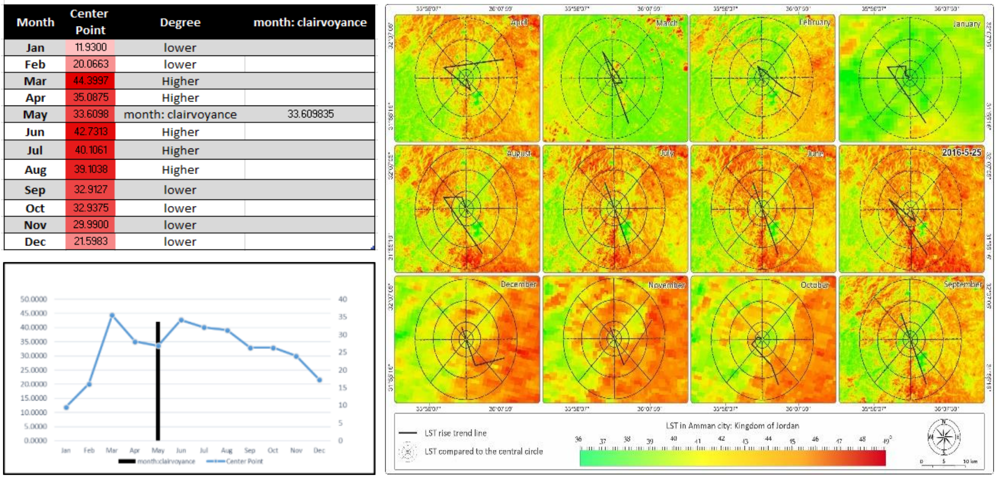

Month	Center Point	Degree	month: clairvoyance
Jan	11.9300	lower	
Feb	20.0663	lower	
Mar	44.3997	Higher	
Apr	35.0875	Higher	
May	33.6098	month: clairvoyance	33.609835
Jun	42.7313	Higher	
Jul	40.1061	Higher	
Aug	39.1038	Higher	
Sep	32.9127	lower	
Oct	32.9375	lower	
Nov	29.9900	lower	
Dec	21.5983	lower	

Figure (4): Monthly Temporal Maps of LST Changes Compared to the month in which clairvoyance occurred in the city of Amman

It is also evident that the number of months recording lower temperatures throughout the year is greater than the number of months recording higher temperatures. On the other hand, the highest recorded temperature was in March, reaching 44.3997, while the lowest recorded temperature was in January, reaching 11.93.

Descriptive Statistics for Amman Data:

Table (3) reveals that the average LST for the months in the Amman region throughout the year was 32.0366 with a standard deviation of 9.79981. The median value was 33.265, indicating that half of the year experiences LST reaching 33.265. Furthermore, Table (4) regarding the Kolmogorov-Smirnov normality test demonstrates that the data follows a normal distribution, with a significance value of 0.368 and 0.189 (sig > 0.05). Therefore, we accept the null hypothesis and reject the alternative hypothesis, indicating that the data follows a normal distribution.

Table (3): Descriptive statistics for LST in the city of Amman

Descriptives				
Amman			Statistic	Std. Error
	Mean		32.0366	2.82896
	95% Confidence Interval for Mean	Lower Bound	25.8101	
		Upper Bound	38.2631	
	5% Trimmed Mean		32.4668	
	Median		33.265	
	Variance		96.036	
	Std. Deviation		9.79981	
	Minimum		11.93	
	Maximum		44.4	
	Range		32.47	
	Interquartile Range		16.16	
	Skewness		-0.808	0.637
	Kurtosis		0.053	1.232

Table (4): the Kolmogorov-Smirnov normality test in the city of Amman

Tests of Normality						
Amman	Kolmogorov-Smirnov[a]			Shapiro-Wilk		
	Statistic	df	Sig.	Statistic	df	Sig.
	0.202	12	0.189	0.929	12	0.368

Moscow

As shown in Figure (5), the Russian capital presents a different scenario compared to the previous regions. On one hand, the LST in the Moscow region during the following months (March, April, May, July, August, September, October, November, and December) records higher levels compared to the month in which clairvoyance occurred (June). Conversely, the months of January and February register lower levels of LST compared to the month in which clairvoyance occurred (June). It is evident that most months throughout the year record higher LST levels than the month in which clairvoyance occurred. In summary, the highest recorded value was in May and November, reaching 46.0246, while the lowest recorded temperature was in February, reaching -8.05.

Descriptive Statistics for Moscow Data:

Table (5) reveals that the average LST for the months in the Moscow region throughout the year was 24.086, with a standard deviation of 18.95573. The median value was 28.92, indicating that half of the year experiences LST reaching 28.92.

Month	Center Point	Degree	month:clairvoyance
Jan	-6.1333	lower	
Feb	-8.0500	lower	
Mar	33.9617	Higher	
Apr	15.0878	Higher	
May	46.0246	Higher	
Jun	4.5100	month:clairvoyance	4.51001
Jul	33.6500	Higher	
Aug	32.3700	Higher	
Sep	25.4700	Higher	
Oct	41.9967	Higher	
Nov	46.0246	Higher	
Dec		Higher	

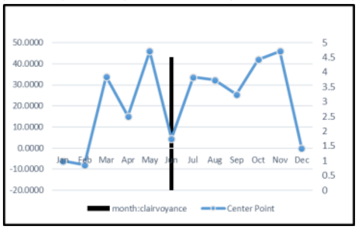

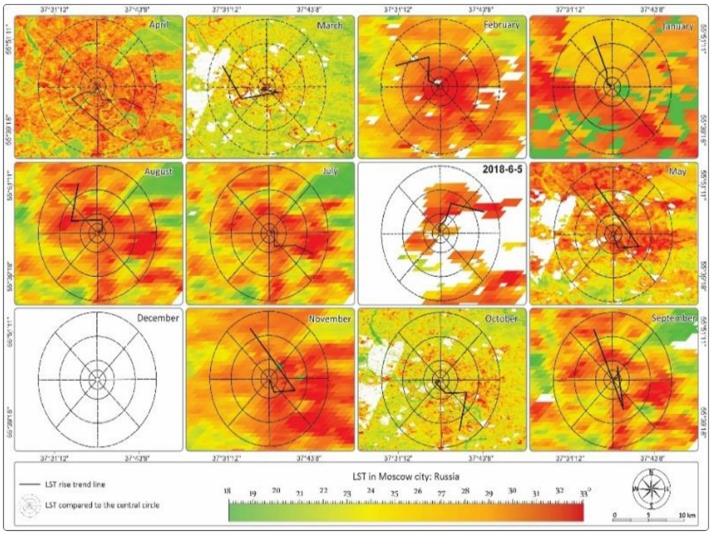

Figure (5): Monthly Temporal Maps of LST Changes Compared to the month in which clairvoyance occurred in Moscow

Table (5): Descriptive statistics for LST in the city of Moscow

Descriptives				
Moscow			**Statistic**	**Std. Error**
	Mean		**24.0806**	**5.47205**
	95% Confidence Interval for Mean	**Lower Bound**	**12.0367**	
		Upper Bound	**36.1245**	
	5% Trimmed Mean		**24.6467**	
	Median		**28.92**	
	Variance		**359.32**	
	Std. Deviation		**18.95573**	
	Minimum		**-8.05**	
	Maximum		**46.02**	
	Range		**54.07**	
	Interquartile Range		**32.83**	
	Skewness		**-0.636**	**0.637**
	Kurtosis		**-0.81**	**1.232**

Furthermore, Table (6) regarding the Kolmogorov-Smirnov normality test demonstrates that the data follows a normal distribution, with a significance value of 0.187 and 0.200 (sig > 0.05). Therefore, we accept the null hypothesis and reject the alternative hypothesis, indicating that the data follows a normal distribution.

- ***Al-Taif***

As indicated in Figure (6), the LST in the Al-Taif region during the following months (March, June, August, September, and October) records higher levels compared to the month in which clairvoyance occurred (May). Conversely, the months of January, February, April, July, November, and December register lower levels of LST compared to the month in which clairvoyance occurred (May). It is also apparent that there is a balance in the number of months throughout the year that record both lower and higher temperatures compared to the month in which clairvoyance occurred. Therefore, the highest recorded value was in June, reaching 39.7040, while the lowest recorded temperature was in January, averaging 22.8540.

Table (6): the Kolmogorov-Smirnov normality test in the city of Moscow

Tests of Normality						
Moscow	Kolmogorov-Smirnov[a]			Shapiro-Wilk		
	Statistic	df	Sig.	Statistic	df	Sig.
	0.169	12	,200*	0.906	12	0.187

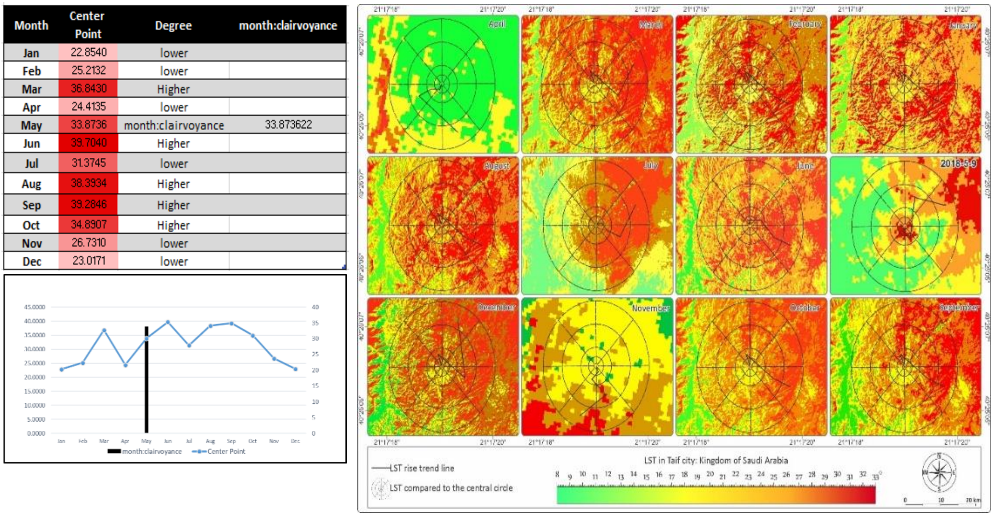

Figure (6): Monthly Temporal Maps of LST Changes Compared to the month in which clairvoyance occurred in Al-Taif

Descriptive Statistics for Al-Taif Data:

Table (7) reveals that the average LST for the months in the Al-Taif region throughout the year was 31.3798, with a standard deviation of 6.60631. The median value was 32.62, indicating that half of the year experiences LST reaching 32.62. Furthermore, Table (8) regarding the Kolmogorov-Smirnov normality test demonstrates that the data follows a normal distribution, with a significance value of 0.096 and 0.200 (sig > 0.05). Therefore, we accept the null hypothesis and reject the alternative hypothesis, indicating that the data follows a normal distribution.

Table (7): Descriptive Statistics for LST in the city of Al-Taif

Descriptives				
			Statistic	Std. Error
Al-Taif	Mean		31.3798	1.90708
	95% Confidence Interval for Mean	Lower Bound	27.1823	
		Upper Bound	35.5772	
	5% Trimmed Mean		31.3914	
	Median		32.62	
	Variance		43.643	
	Std. Deviation		6.60631	
	Minimum		22.85	
	Maximum		39.7	
	Range		16.85	
	Interquartile Range		13.39	
	Skewness		-0.092	0.637
	Kurtosis		-1.829	1.232

Table (8): the Kolmogorov-Smirnov normality test in the city of Al-Taif

Tests of Normality						
	Kolmogorov-Smirnov[a]			Shapiro-Wilk		
Al-Taif	Statistic	df	Sig.	Statistic	df	Sig.
	0.176	12	,200*	0.883	12	0.096

- **Relationships Between LST and Distance from the Central Point in the Clairvoyantly Perceived Regions and Surrounding Areas.**

- ***Abu Dhabi:***

According to Figure (7) representing LST observed on January 31, 2022, it is evident that the LST in the central area is higher than the surrounding circles, a pattern observed in all months except for December and February when the center shows lower temperatures than C1 and C2, respectively. As indicated in Table (9) concerning the Mann-Whitney test, the p-values for all the LST centers are greater than 0.05. This suggests that there are no statistically significant differences between the central point and the surrounding points, indicating relative balance between the central point and its neighboring points.

- ***Amman:***

According to Figure (8) representing LST observed on May 25, 2016, it becomes apparent that the LST in the central area is lower than the surrounding circles starting from C2 approximately. This pattern is observed in all months except for December, where a noticeable increase is observed. As revealed in Table (10) related to the Mann-Whitney test, the p-values for all the LST centers are greater than 0.05. This suggests that there are no statistically significant differences between the central point and the surrounding points, indicating relative balance between the central point and its neighboring points.

Name	Jan Mean	Feb Mean	Mar Mean	Apr Mean	May Mean	Jun Mean	Jul Mean	Aug Mean	Sep Mean	Oct Mean	Nov Mean	Dec Mean	Total Year Average
Center point	51.1615	22.6800	47.0597	51.0599	51.1094	57.3993	51.5923	56.0731	56.0731	50.0668	26.2986	20.8406	45.1178
C1 Average	51.1545	23.8667	46.9658	50.5134	50.5812	56.8518	51.0650	55.7787	55.7787	49.8284	26.4084	21.4348	45.0189
C2 Average	51.0853	22.9109	46.7326	50.2248	50.2355	56.5373	50.7716	55.5763	55.5763	49.6145	26.3926	21.5855	44.7703
C3 Average	50.0103	21.1722	45.4615	48.3030	48.2824	54.7248	49.0051	54.0621	54.0621	47.9737	24.0736	20.0940	43.1021
C4 Average	49.6644	20.2320	45.0223	47.6120	47.6503	54.0809	48.4240	53.5643	53.5643	47.5563	23.5063	19.7506	42.5523

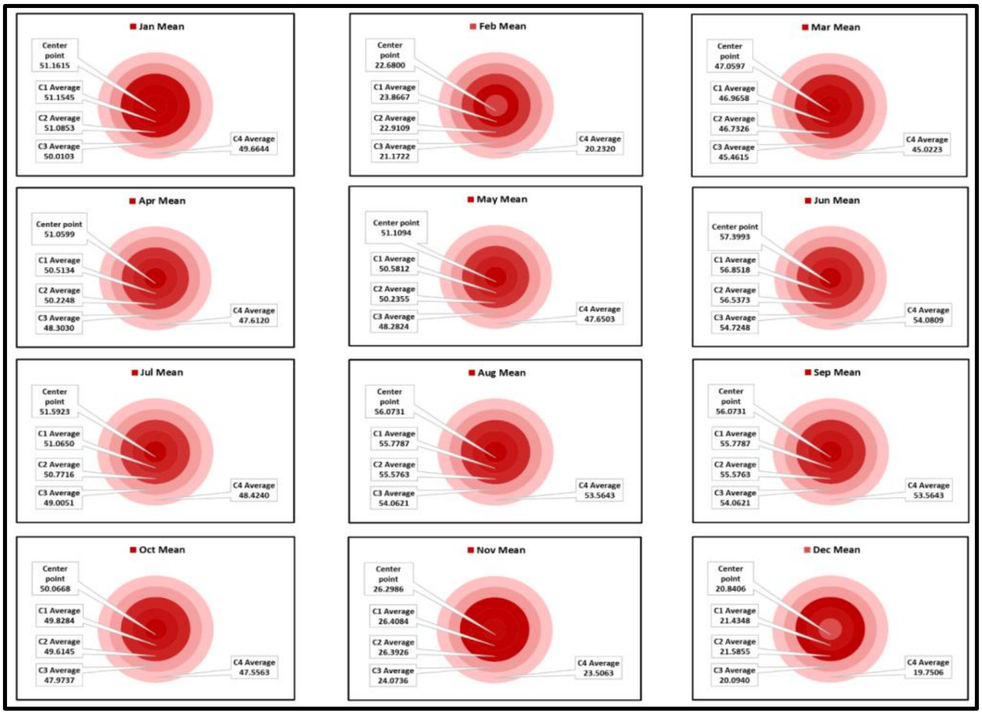

Figure (7): Relationships Between LST and Distance from the Central Point and Surrounding Areas in Abu Dhabi

Table (9): The Mann-Whitney test for LST Between the Central Point and Surrounding Areas in Abu Dhabi

	U	Expected Value	Variance (U)	p-value	alpha
C1 Average	76,000	72,000	300,000	0,840	0,05
C2 Average	62,000	72,000	300,000	0,583	0,05
C3 Average	60,000	72,000	300,000	0,507	0,05
C4 Average	59,000	72,000	300,000	0,470	0,05

- ***Moscow:***

According to Figure (9) representing LST observed on June 5, 2018, it becomes apparent that the LST in the central area is relatively higher than the surrounding circles, with variations. This pattern is observed in almost all months, except for January and February when the center shows relatively lower temperatures. As shown in Table (11) related to the Mann-Whitney test, the p-values for all the LST centers in the Moscow region are greater than 0.05. This suggests that there are no statistically significant differences between the central point and the surrounding points, indicating relative balance between the central point and its neighboring points.

Name	Jan Mean	Feb Mean	Mar Mean	Apr Mean	May Mean	Jun Mean	Jul Mean	Aug Mean	Sep Mean	Oct Mean	Nov Mean	Dec Mean	Total Year Average
Center point	11.9300	20.0663	44.3997	35.0875	33.6098	42.7313	40.1061	39.1038	32.9127	32.9375	29.9900	21.5983	32.0394
C1 Average	11.8656	20.1275	44.2218	34.2019	32.6619	41.8385	39.3353	38.1693	31.9865	34.5261	30.5973	21.1391	31.7226
C2 Average	12.4689	20.7413	44.4191	36.0846	34.0951	43.2681	40.7831	39.8198	33.6788	36.2144	31.9852	21.9097	32.9557
C3 Average	12.7650	21.7826	44.6588	37.1436	34.4167	43.4427	41.1092	41.0186	34.5236	36.7892	31.6752	21.7301	33.4213
C4 Average	12.9826	22.3070	44.5831	37.9281	34.7004	43.8381	41.5687	42.4072	35.4191	37.0974	31.6885	21.6514	33.8476

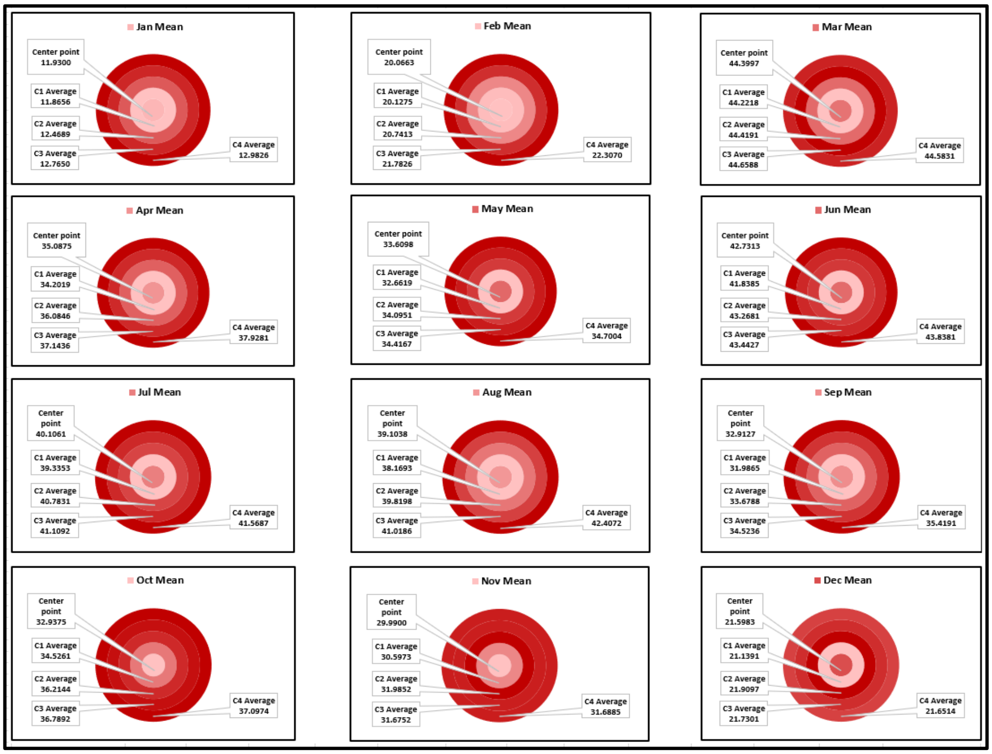

Figure (8): Relationships Between LST and Distance from the Central Point and Surrounding Areas in Amman

Table (10): The Mann-Whitney test for LST Between the Central Point and Surrounding Areas in Amman

	U	Expected Value	Variance (U)	p-value	alpha
C1 Average	76,000	72,000	300,000	0,840	0,05
C2 Average	62,000	72,000	300,000	0,583	0,05
C3 Average	60,000	72,000	300,000	0,507	0,05
C4 Average	59,000	72,000	300,000	0,470	0,05

Al-Taif:

From Figure (10) representing LST observed on May 9, 2018, it is clear that the temperature in the central circle surrounding the clairvoyance area varies. It is neither consistently higher nor consistently lower than the surrounding areas in general. Additionally, the temperature in the smallest circle, which represents the clairvoyance area, is also variable, sometimes higher and sometimes lower than the surrounding areas in all months.

Name	Jan Mean	Feb Mean	Mar Mean	Apr Mean	May Mean	Jun Mean	Jul Mean	Aug Mean	Sep Mean	Oct Mean	Nov Mean	Dec Mean	Total Year Average
Center point	-6.1333	-8.0500	33.9617	15.0878	46.0246	4.5100	33.6500	32.3700	25.4700	41.9967	46.0246		24.0829
C1 Average	-5.8628	-5.0325	33.6150	14.1839	45.7031	2.2825	25.0662	23.8662	18.9900	41.7067	45.7031		21.8383
C2 Average	-5.4881	-8.2380	33.4122	13.9299	44.9265	3.9710	33.1065	31.8344	25.2856	41.6543	44.9265		23.5746
C3 Average	-5.6204	-9.2279	33.2188	13.4401	44.1018	5.0061	32.5220	31.5529	25.5419	41.7227	44.1018		23.3054
C4 Average	-6.3679	-10.1078	33.0198	12.8289	43.9226	3.7494	31.7096	31.0547	25.3436	41.6745	43.9226		22.7955

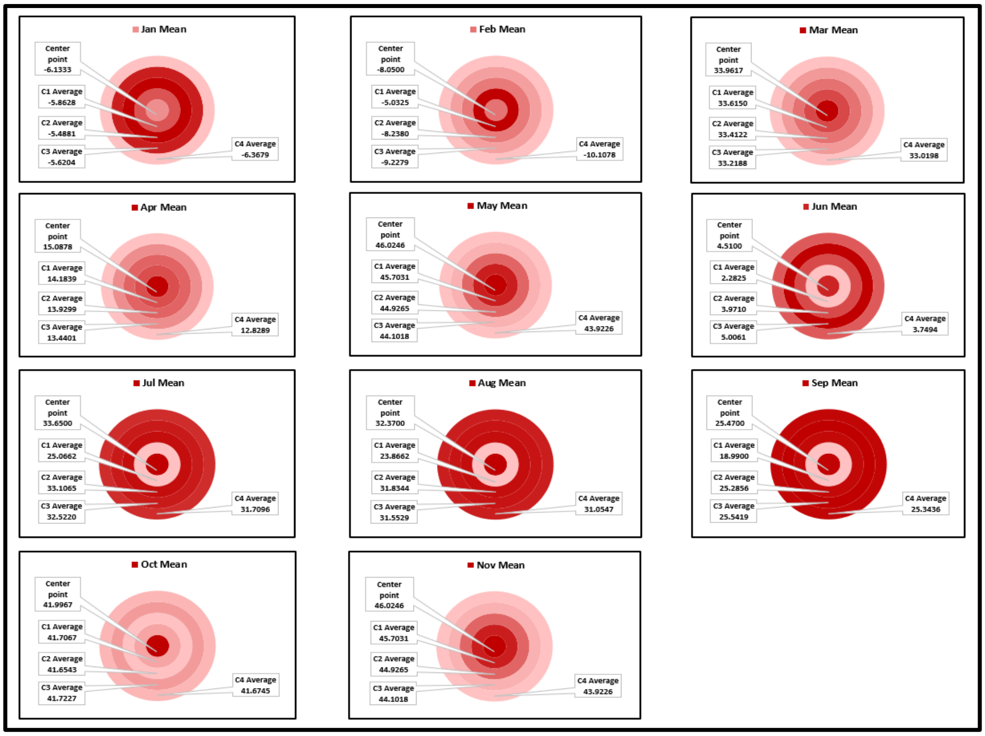

Figure (9): Relationships Between LST and Distance from the Central Point and Surrounding Areas in Moscow

Table (11): The Mann-Whitney test for LST Between the Central Point and Surrounding Areas in Moscow

	U	Expected Value	Variance (U)	p-value	alpha
C1 Average	**68,000**	**60,500**	**231,655**	**0,646**	**0,05**
C2 Average	**67,000**	**60,500**	**231,655**	**0,693**	**0,05**
C3 Average	**65,000**	**60,500**	**231,655**	**0,793**	**0,05**
C4 Average	**69,000**	**60,500**	**231,655**	**0,599**	**0,05**

Table (12) related to the Mann-Whitney test indicate that the p-values for all the LST centers in the Al-Taif region are greater than 0.05. This suggests that there are no statistically significant differences between the central point and the surrounding points, indicating relative balance between the central point and its neighboring points.

Name	Jan Mean	Feb Mean	Mar Mean	Apr Mean	May Mean	Jun Mean	Jul Mean	Aug Mean	Sep Mean	Oct Mean	Nov Mean	Dec Mean	Total Year Average
Center point	22.8540	25.2132	36.8430	24.4135	33.8736	39.7040	31.3745	38.3934	39.2846	34.8907	26.7310	23.0171	31.3827
C1 Average	22.8456	25.0924	36.5762	24.3294	34.8614	39.3318	31.4956	38.0920	39.0470	34.8440	26.7979	23.1918	31.3754
C2 Average	23.1982	25.4787	36.7066	24.3374	32.5676	39.2746	31.6234	38.1099	39.2350	35.1995	27.1638	23.3144	31.3507
C3 Average	24.5362	26.3470	37.8656	24.2705	30.4687	39.5452	31.6911	38.8139	40.1992	36.6221	27.6141	24.1226	31.8413
C4 Average	24.2606	25.5916	37.5765	24.4134	30.3223	38.9751	30.3252	38.2145	39.8234	36.5501	28.3652	23.6405	31.5049

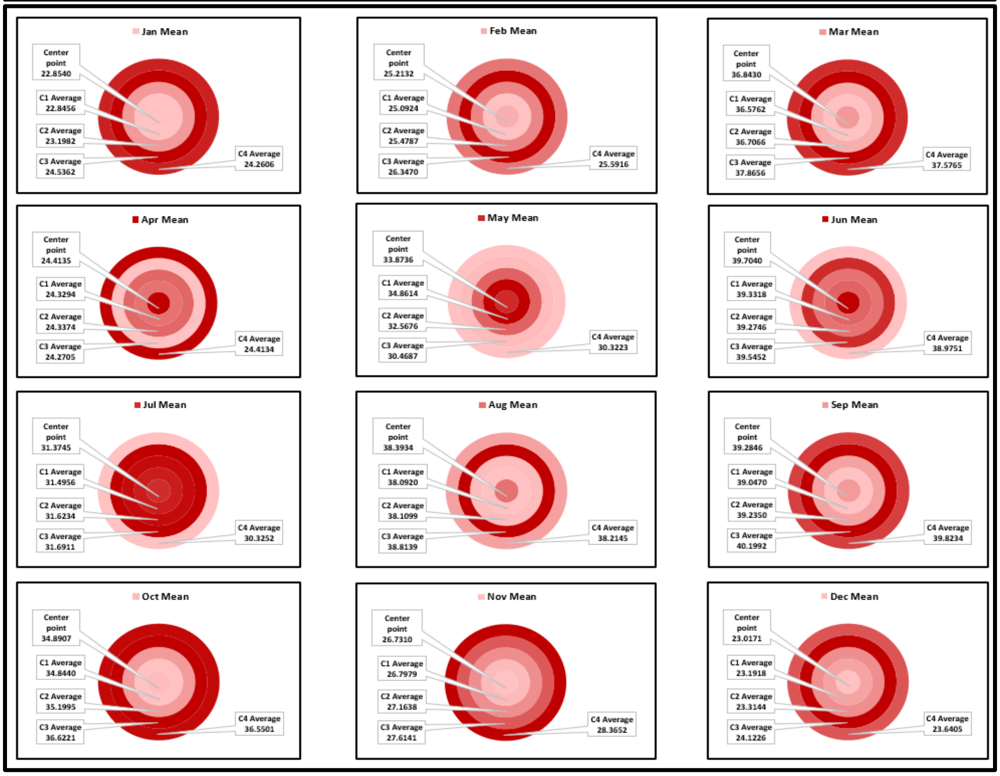

Figure (10): Relationships Between LST and Distance from the Central Point and Surrounding Areas in Al-Taif

Table (12): The Mann-Whitney test for LST Between the Central Point and Surrounding Areas in Al-Taif

	U	Expected Value	Variance (U)	p-value	alpha
C1 Average	74,000	72,000	300,000	0,931	0,05
C2 Average	72,000	72,000	300,000	1,000	0,05
C3 Average	67,000	72,000	300,000	0,795	0,05
C4 Average	71,000	72,000	300,000	0,977	0,05

- **Daily Temporal Variations of LST in the Central Point within the Clairvoyantly Perceived Regions:**

Comparison of Observed LST on Days Before and After Clairvoyance Using a Descriptive Approach for Recorded Values and Their Graphic Representation. Additionally, the Mann-Whitney U test, a non-parametric test, was employed to evaluate temperature differences before and after the clairvoyance event. Below is a presentation of the results:

- ***Abu Dhabi:***

From Figure (11), representing LST on the days before and after clairvoyance, it is evident that the LST observed on the day on which clairvoyance occurred is the highest compared to the temperatures observed before and after it, with a relative convergence with the day following clairvoyance, as indicated in this figure.

Hypothesis testing for statistically significant differences in LST on the days before and after clairvoyance in the Abu Dhabi region:

According to Table (13), the p-value for the Mann-Whitney test is 0.651, which is greater than 0.05. This suggests that there are no statistically significant differences between the days before and after clairvoyance, indicating a relative stability in LST before and after clairvoyance.

Date	Center Point	Degree	month:clairvoyance
24/01/2022	22.4100	lower	
30/01/2022	19.2500	lower	
31/01/2022	51.1615	month:clairvoyance	51.161486
01/02/2022	45.8335	lower	
02/02/2022	22.0000	lower	
06/02/2022	20.8250	lower	

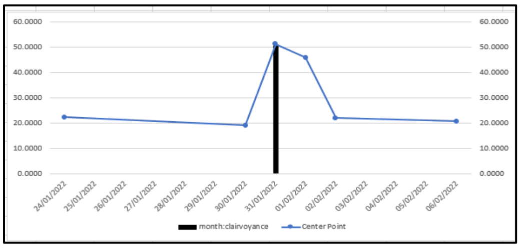

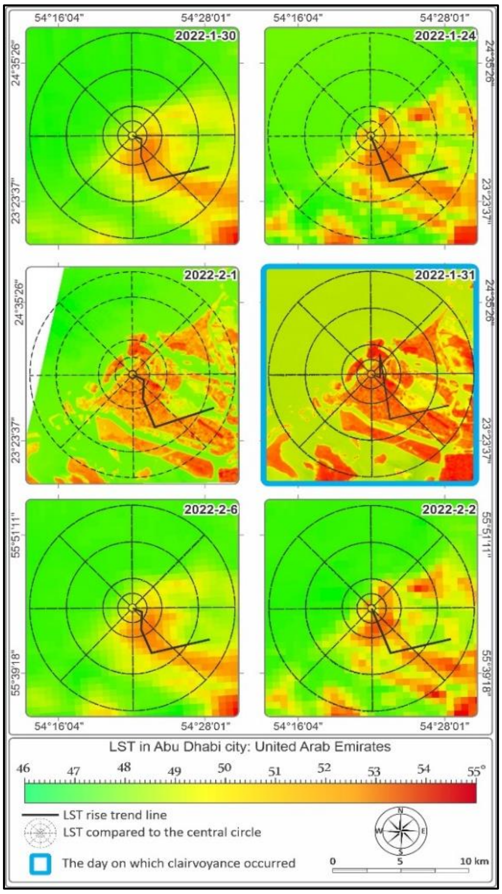

Figure (11): Daily Temporal Maps of LST Changes at the Central Point Before and After the Occurrence of Clairvoyance in the City of Abu Dhabi.

Table (13): P-Values from Mann-Whitney Test for LST before/after the occurrence of Clairvoyance in Abu Dhabi

U	**2,000**
Expected value	**2,000**
Variance (U)	**1,667**
p-value(one-tailed)	**0,651**
alpha	**0,05**

- ***Amman:***

From Figure (12), representing LST on the days before and after clairvoyance in Amman, it is evident that the LST observed on the day on which clairvoyance occurred is the lowest compared to the temperatures observed before and after it, with a relative convergence with all observed temperatures and the day on which clairvoyance occurred, as indicated in this figure.

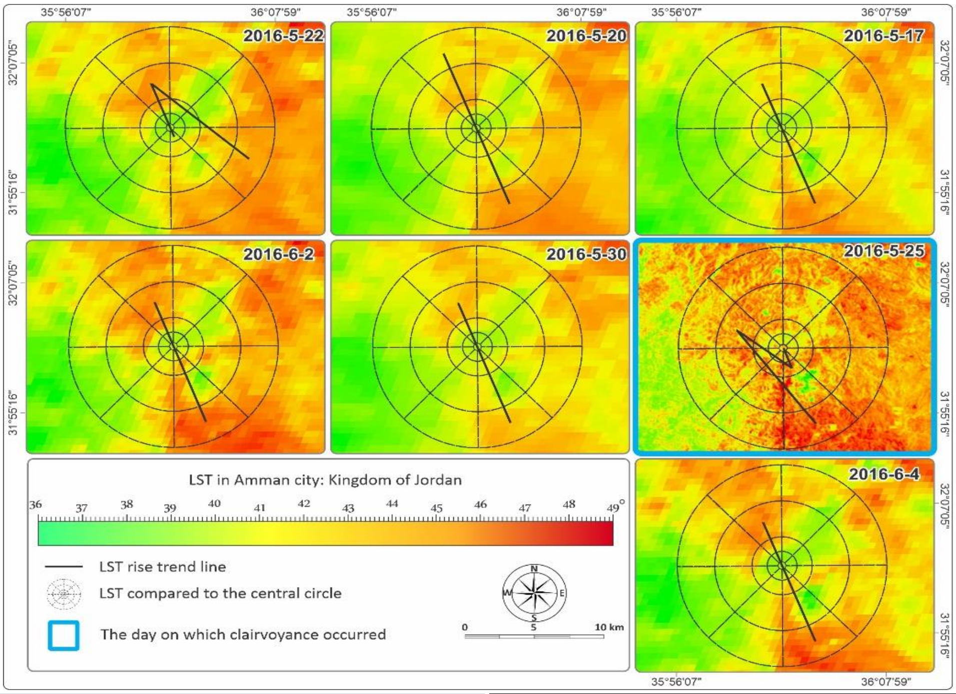

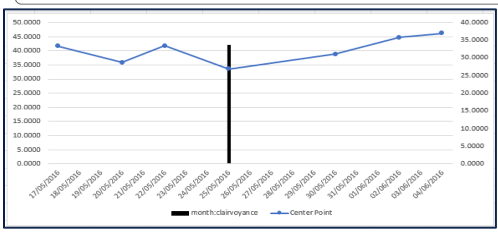

Date	Center Point	Degree	month:clairvoyance
17/05/2016	41.5500	Higher	
20/05/2016	35.8500	Higher	
22/05/2016	41.7900	Higher	
25/05/2016	33.6098	month:clairvoyance	33.609835
30/05/2016	38.8300	Higher	
02/06/2016	44.6700	Higher	
04/06/2016	46.1100	Higher	

Figure (12): Daily Temporal Maps of LST Changes at the Central Point Before and After the Occurrence of Clairvoyance in Amman

Hypothesis testing for statistically significant differences in LST on the days before and after clairvoyance in Amman:

According to Table (14), the p-value for the Mann-Whitney test is 0.877, which is greater than 0.05. This suggests that there are no statistically significant differences between the days before and after clairvoyance, indicating a relative stability in LST before and after clairvoyance.

Table (14): P-Values from Mann-Whitney Test for LST before/after the occurrence of Clairvoyance in Amman

U	**1,000**
Expected value	**2,000**
Variance (U)	**1,667**
p-value (one-tailed)	**0,877**
alpha	**0,05**

- ***Moscow:***

From Figure (13), representing LST on the days before and after clairvoyance in Moscow, it is evident that the LST observed on the day on which clairvoyance occurred is the lowest compared to the temperatures observed before and after it. However, there is a noticeable variation with the temperatures observed on the day on which clairvoyance occurred, as shown in this figure.

Hypothesis testing for statistically significant differences in LST on the days before and after clairvoyance in Moscow:

According to Table (15), the p-value for the Mann-Whitney test is 0.331, which is greater than 0.05. This suggests that there are no statistically significant differences between the days before and after clairvoyance, indicating a relative stability in LST before and after clairvoyance in Moscow.

- ***Taif:***

From Figure (14), representing LST on the days before and after clairvoyance in Taif, it is evident that the LST observed on the day on which clairvoyance occurred is the lowest compared to the temperatures observed before and after it. However, there is a noticeable variation with the temperatures observed on the day on which clairvoyance occurred, as shown in this figure.

Hypothesis testing for statistically significant differences in LST on the days before and after clairvoyance in Taif:

According to Table (16), the p-value for the Mann-Whitney test is 0.651, which is greater than 0.05. This suggests that there are no statistically significant differences between the days before and after clairvoyance, indicating a relative stability in LST before and after clairvoyance in Taif.

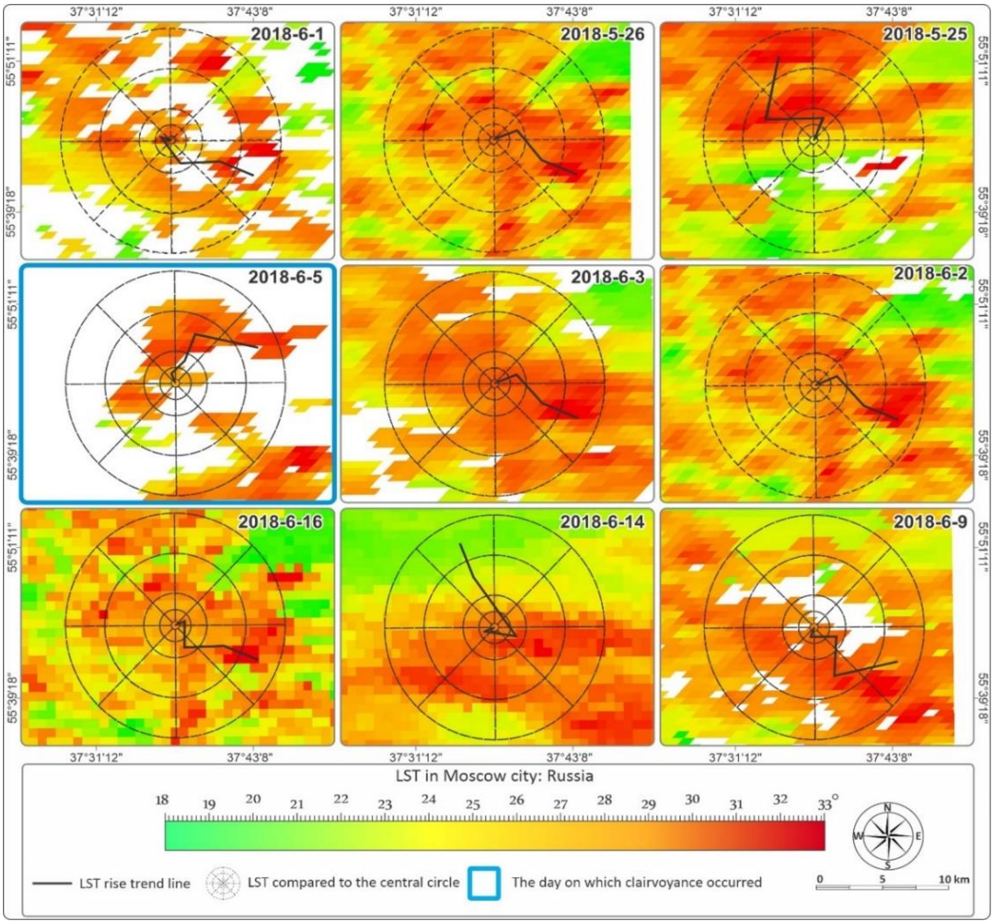

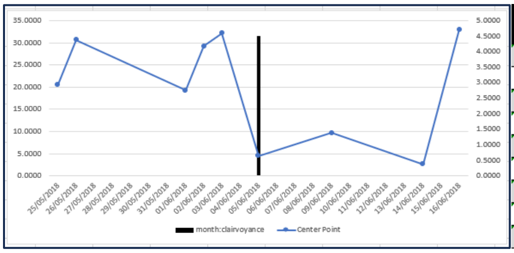

Date	Center Point	Degree	month:clairvoyance
25/05/2018	20.5900	Higher	
26/05/2018	30.6100	Higher	
01/06/2018	19.2300	Higher	
02/06/2018	29.2500	Higher	
03/06/2018	32.1500	Higher	
05/06/2018	4.5100	month:clairvoyance	4.51001
09/06/2018	9.6900	Higher	
14/06/2018	2.6520	lower	
16/06/2018	32.9360	Higher	

Figure (13): Daily Temporal Maps of LST Changes at the Central Point before and after the Occurrence of Clairvoyance in Moscow

Table (15): P-Values from Mann-Whitney Test for LST before/after the occurrence of Clairvoyance in Moscow

U	**6,000**
Expected value	**4,500**
Variance (U)	**5,250**
p-value (one-tailed)	**0,331**
alpha	**0,05**

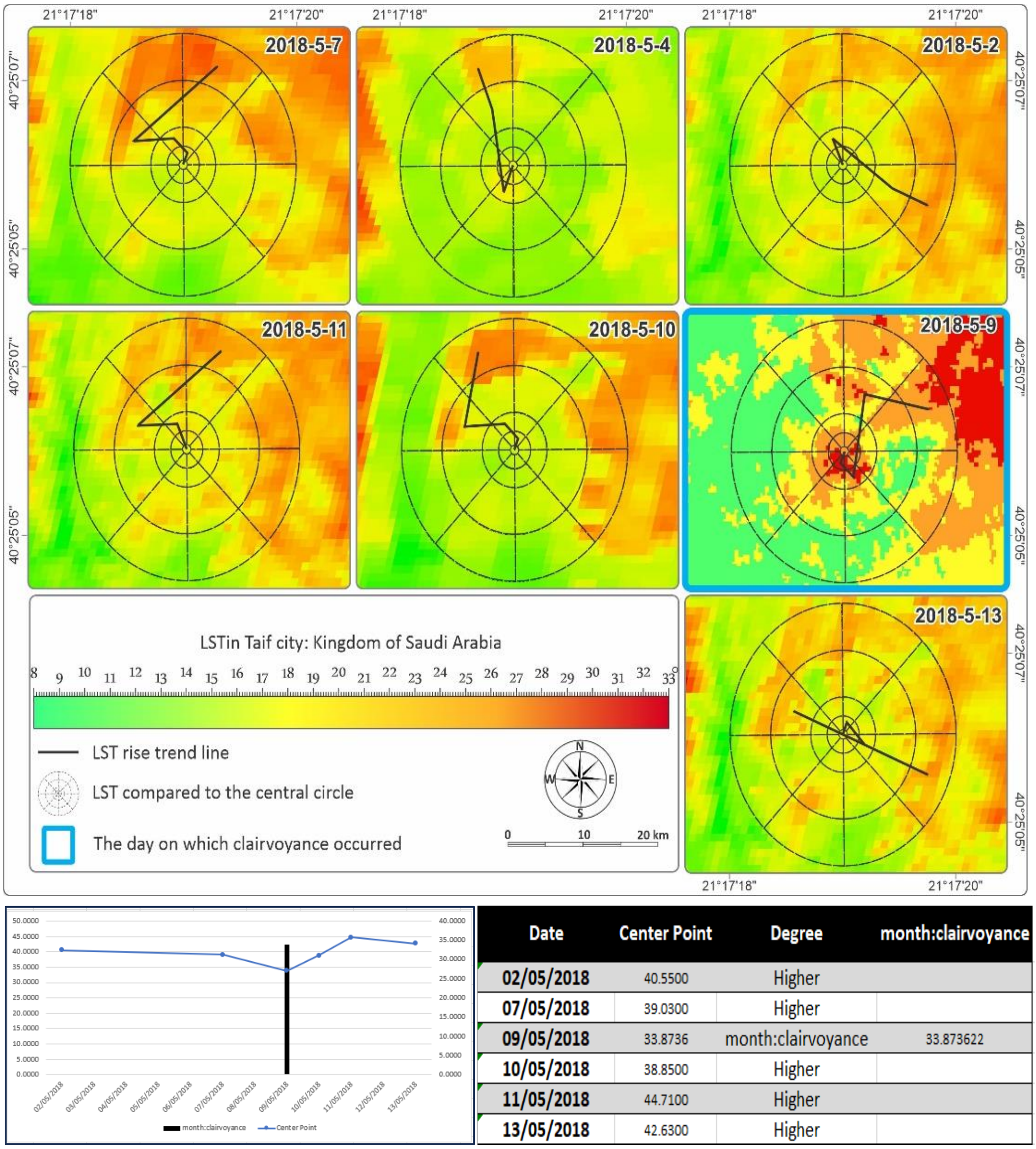

Date	Center Point	Degree	month:clairvoyance
02/05/2018	40.5500	Higher	
07/05/2018	39.0300	Higher	
09/05/2018	33.8736	month:clairvoyance	33.873622
10/05/2018	38.8500	Higher	
11/05/2018	44.7100	Higher	
13/05/2018	42.6300	Higher	

Figure (14): Daily Temporal Maps of LST Changes at the Central Point Before and After the Occurrence of Clairvoyance in Al-Taif

Table (16): P-Values from Mann-Whitney Test for LST before/after the occurrence of Clairvoyance in Al-Taif

U	**2,000**
Expected value	**2,000**
Variance (U)	**1,667**
p-value (one-tailed)	**0,651**
alpha	**0,05**

Comparing Clairvoyance Days with Other Months for All Cities:

According to Table (17), the LST observed on the day on which clairvoyance occurred does not constitute an extreme maximum or minimum value for any of the cities. Thus, it falls within the extreme values range for months throughout the year.

However, there is a variation in the annual average LST for each city. The lowest average temperature was recorded in Moscow at 24.0806 degrees Celsius, while the highest was recorded in Abu Dhabi at 45.1179 degrees Celsius. Finally, the average LST for both Amman and Taif falls within the range of 30 to 32.5 degrees Celsius.

Table (17): Spatial LST Changes on the Day of Clairvoyance in All Study Areas

Cities	Incidence Month	Minimum	Maximum	Mean	Status
Abu Dhabi	51,1615	20,84	57,40	45,1179	within the field
Amman	33,60	11,93	44,40	32,0366	within the field
Moscow	4,51	-8,05	46,02	24,0806	within the field
Al-Taif.	33,87	22,85	39,70	31,3798	within the field

- **The Impact of Clouds on LST in the Clairvoyantly Perceived Regions.**

Returning to the satellite imagery in the clairvoyance regions, it became evident that both Taif and Amman, as well as Abu Dhabi, were characterized by clear skies during the day on which clairvoyance occurred. This contributed to the accurate retrieval of LSTs. In contrast, Moscow was clouded over on the day on which clairvoyance occurred, as seen in Figure (15), which affected the quality of the extracted data. It is well-known that clouds are a natural factor beyond human control.

- **Analysis of the LST Gradient Compared to the day on which clairvoyance occurred.**

From the descriptive analysis of Figures (3-6), it became clear that the LST trend line on the day on which clairvoyance occurred in Moscow, Abu Dhabi, and Taif moved in a specific direction, which is eastward. However, Amman deviated slightly towards the southeast, and there was no significant influence observed from the north, south, or west.

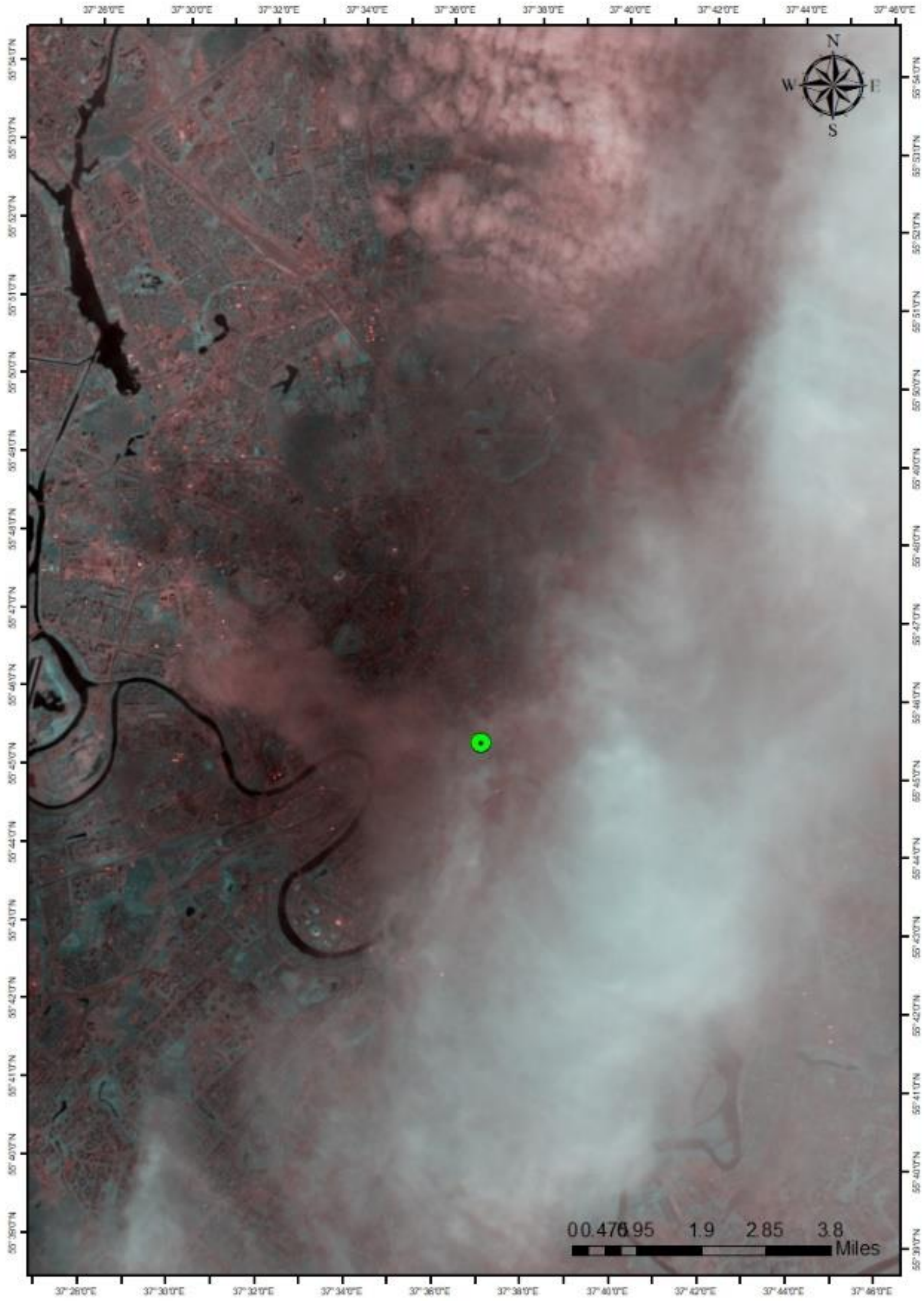

Figure. (15): An image showing The Impact of Clouds on the Moscow region on 6/5/2018

Discussion:

From the results of the study, it became evident that all LST observed on the day on which clairvoyance occurred do not constitute extreme maximum or minimum values for each of the cities. This contradicts studies by Serena and Roney (2010) and El-Borie (2021), which indicated that cosmic phenomena such as Schumann resonance and Earth's magnetic field influence cosmic temperatures and subsequently affect clairvoyance abilities. It was initially expected that there would be a correlation between LST and clairvoyance. In other words, when cosmic phenomena affect cosmic temperatures, it would follow that there would be an impact on the surface temperature, which, in turn, would affect clairvoyance abilities. However, this hypothesis was not supported by our study. Thus, it can be concluded that there is no significant thermal anomaly in any place clairvoyantly perceived compared to other months.

The tables presented in the results provide a comparative descriptive image of the surface temperature for the central observed point and the surrounding areas. Visually, no significant differences were observed except in some months where the central point recorded higher surface temperatures, but without significant convergence between it and the other points. These findings were further validated through the Mann-Whitney test, which showed no statistically significant differences between the central point and the surrounding points within each region. This indicates a relative balance between the central point and its adjacent points.

Moreover, the tables illustrate differences between the observed LST and the days before and after clairvoyance. At times, it was lower, and at other times, it was higher, with occasional convergence and divergence. Again, these results were confirmed by the Mann-Whitney test, which showed no statistically significant differences at the 0.05 level between the days before and after the day on which clairvoyance occurred. This suggests a relative equilibrium in LST for the days surrounding the observed LST on the day on which clairvoyance occurred.

Implications and Applications:

The study aimed to investigate if there is a correlation between land surface temperature and clairvoyance occurrence. The study's methods and findings can potentially inform future research on the relationship between cosmic phenomena and human behavior, anomalies, and interdisciplinary studies that aim to understand the impact of environmental factors on human abilities. The findings of the study highlight the importance of empirical research to test and challenge existing theories and assumptions in various fields. In particular, identifying the types of radiations involved enables the implementation of proactive measures to mitigate their adverse effects and harness their potential for various applications. This profound insight serves as a sturdy basis for practical initiatives geared towards environmental preservation and ensuring human safety, thereby contributing to the protection of humanity from natural disasters and human-related challenges.

Conclusion:

In this study, land surface temperature (LST) across several clairvoyantly perceived regions is analyzed and extrapolated utilizing a diverse range of imagery from various satellite sources. This endeavor aimed to shed light on the temporal and spatial variations in LST within these areas (Moscow, Taif, Amman, and Abu Dhabi). One of the most significant revelations arising from this study is the absence of substantial thermal anomalies during clairvoyance events, indicating their similarity to other months. Furthermore, our research unveiled a relative balance between the central point and its surrounding areas within each clairvoyantly perceived region, emphasizing the harmonious dynamics at play. Lastly, the statistical analysis demonstrated no significant differences at the 0.05 level between the days before and after clairvoyance events, suggesting a state of relative equilibrium in LST during the days surrounding these extraordinary occurrences.

References:

- *Achmad, A., & Muftiadi, M. (2019, October). The relationship between land surface temperature and water index in the urban area of a tropical city. In IOP Conference Series: Earth and Environmental Science (Vol. 365, No. 1, p. 012013). IOP Publishing.*

- *Al-Najdawi, Lina (2022). "Assessing the Efficiency of Security Center Distribution in Amman City Using Geographic Information Systems (GIS)." Unpublished Master's Thesis, Mutah University. Mutah.*

- *Comprehensive Urban Vision Report for the city of Taif (2021). Ministry of Municipal and Rural Affairs.* https://unhabitat.org/sites/default/files/2020/04/taif.pdf.

- *El-Borie, M. A., Thabet, A. A., El-Mallah, E. S., Abd El-Zaher, M., & Bishara, A. A. (2021). The combined influences for solar-geomagnetic* *activities and the atmospheric circulation NAO on global surface temperatures. Indian Journal of Physics, 95, 1041-1049.*

- *Girona, T., Realmuto, V., & Lundgren, P. (2021). Large-scale thermal unrest of volcanoes for years prior to eruption. Nature Geoscience, 14(4), 238-241.*
- *Huda, D. N., & Shidiq, I. P. A. (2020, July). Spatiotemporal analysis land surface temperature in relation to earthquake occurrence around the cimandiri fault. In IOP Conference Series: Earth and Environmental Science (Vol. 540, No. 1, p. 012069). IOP Publishing.*
- *McCraty, R., & Atkinson, M. (2014). Electrophysiology of intuition: pre-stimulus responses in group and individual participants using a Roulette paradigm. Global advances in health and medicine, 3(2), 16-27.*
- *Morris, R. L. (1978). A survey of methods and issues in ESP research. In Advances in Parapsychological Research: Volume 2: Extrasensory Perception (pp. 7-58). Boston, MA: Springer US.*
- *Mossbridge, J. (2023). Precognition at the boundaries: An empirical review and theoretical discussion. Journal of Anomalous Experience and Cognition, 3(1), 5-41.*
- *O'Shea, M. (2005). The brain: a very short introduction (Vol. 144). Oxford University Press, USA.*
- *Prokofeva, T., Shishkov, V., & Kiriushin, A. (2021). Calcium carbonate accumulations in Technosols of Moscow city. Journal of Soils and Sediments, 21(5), 2049-2058.*
- *Radin, D. I. (2004). Electrodermal presentiments of future emotions. Journal of Scientific Exploration, 18(2), 253-273.*
- *REHMAN, Z. U., Mahar, G. A., Chandio, N. H., Iqbal, M. J., & Kazmi, J. H. (2019). Appraisal of land cover changes in the Upper Sindh through geo-informatics techniques. Sindh University Research Journal-SURJ (Science Series), 51(01), 141-146.*
- *Road, H. and Tw, T. (2008) 'New Insights into the Links between ESP and Geomagnetic Activity', 22(3), pp. 335–358.*
- *Roney-Dougal, S. M., Ryan, A., & Luke, D. (2010). The relationship between local geomagnetic activity, Tibetan Buddhist meditation and psychic awareness: preliminary study.*
- *Ryan, A. (2008). New insights into the links between ESP and*

geomagnetic activity. Journal of Scientific Exploration, 22(3), 335-358.

- *Shah, M., Qureshi, R. U., Khan, N. G., Ehsan, M., & Yan, J. (2021). Artificial Neural Network based thermal anomalies associated with earthquakes in Pakistan from MODIS LST. Journal of Atmospheric and Solar-Terrestrial Physics, 215, 105568.*
- *Spottiswood, J. (no date) 'GEOMAGNETIC FLUCTUATIONS AND FREE RESPONSE ANOMALOUS COGNITION: A NEW UNDERSTANDING', pp. 1–9.*
- *Targ, R., & Puthoff, H. E. (2005). Mind-reach: Scientists look at psychic abilities. Hampton Roads Publishing.*
- *Tariq, A., Siddiqui, S., Sharifi, A., & Shah, S. H. I. A. (2022). Impact of spatio-temporal land surface temperature on cropping pattern and land use and land cover changes using satellite imagery, Hafizabad District, Punjab, Province of Pakistan. Arabian Journal of Geosciences, 15(11), 1045.*
- *Tuszynski, J. A. (2020). From quantum chemistry to quantum biology: A path toward consciousness. Journal of Integrative Neuroscience, 19(4), 687-700.*
- *Weng, Q., Lu, D., & Schubring, J. (2004). Estimation of land surface temperature–vegetation abundance relationship for urban heat island studies. Remote Sensing of Environment, 89, 467−483.*
- *Williams III, G. R. (2016). What Can Consciousness Anomalies Tell Us about Quantum Mechanics? Journal of Scientific Exploration, 30(3).Retrieved from https://journalofscientificexploration.org/index.php/jse/article/view/1001.*
- *Zingrone, N. & Alvarado, C.S. (2015) A brief history of psi, in May, E.C. & Marwaha, S.B. (eds.) Extrasensory Perception: Support, Skepticism, and Science, Volume I — History, Controversy, & Research, Santa Barbara, CA: Praeger Publications (Statistics Center, 2017: Abu Dhabi).*